Supporting Information

For

Synthesis of Mn doped and anatase/rutile mixed-phase TiO_2 nanofibers for high photo activity performance

Fan Fu[1], Yufan Zhang[1], Yan Zhang[1]*, Yuyue Chen[1]*

National Engineering Laboratory for Modern Silk, College of Textile and Clothing Engineering,

Soochow University, Suzhou 215123, People's Republic of China

* Corresponding author: yanzhang86@suda.edu.cn; chenyy@suda.edu.cn

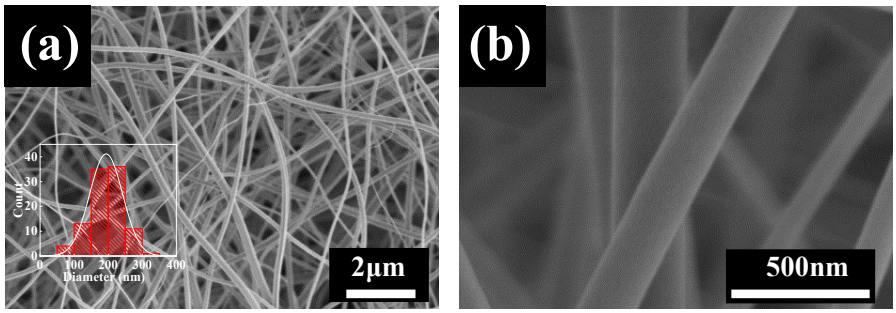

Figure SI 1: (a, b) SEM images of PVP-Mn@TiO_2-0.10 annealed at 600 °C for 1 hour in air with the histograms of diameter distribution analysis.

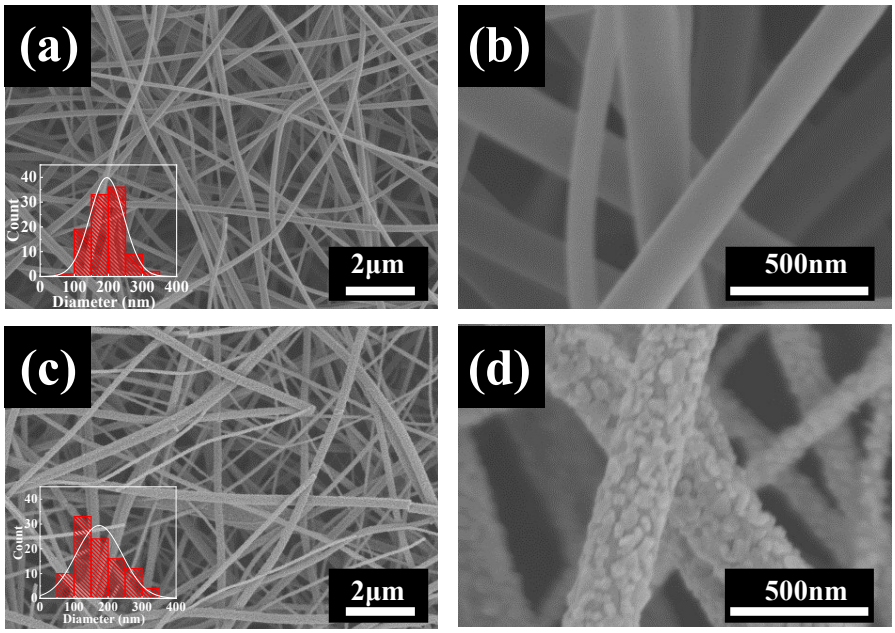

Figure SI 2: SEM images of PVP-Mn@TiO_2-0.10: (a, b) annealed at 450 ^oC for 1 hour under the N_2 atmosphere; (c, d) annealed at 750 ^oC for 1 hour under the N_2 atmosphere with each histograms of diameter distribution analysis.

Table SI 1: The diameter distribution result of PVP-Mn@TiO_2-0.10 after different treatment.

Experimental parameters	**Diameter (nm)**
450 ^oC, 1 h, N_2	195.49±9.80
600 ^oC, 1 h, N_2	189.91±9.80
750 ^oC, 1 h, N_2	173.64±13.31
600 ^oC, 1 h, Air	193.88±9.50

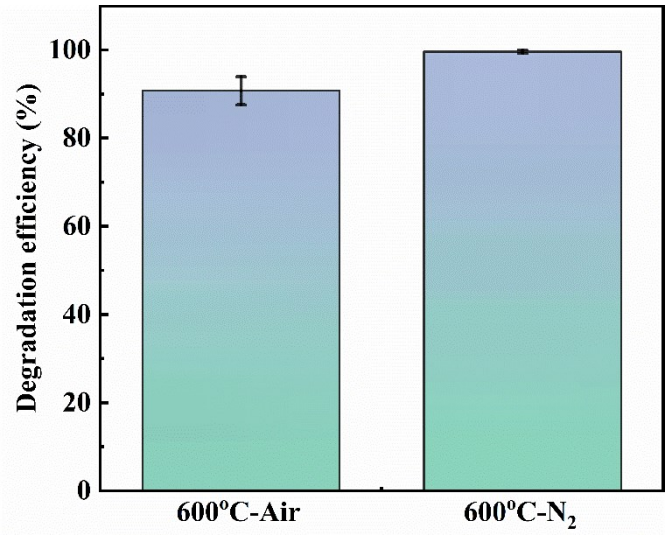

Figure SI 3: Photodegradation efficiency from Mn@TiO_2-0.10 nanofibers synthesized at different conditions.

Table SI 2: Comparison of photocatalytic contaminants removal rate and reuse cycle of various TiO_2 nanofibers based photocatalysts.

Photocatalysts	Light source	Target compound	Removal rate (min^{-1})	Reuse cycle	Ref.
Mn@TiO_2	20 W, 325 nm	Methylene blue	$5.22E^{-2}$	5	This work
Fe_2O_3/TiO_2	500 W Hg lamp	Rhodamine B	$5.00E^{-2}$	1	[1]
BN–Ag/TiO_2	150 W visible light	Methylene blue	$4.65E^{-2}$	4	[2]
$ZnTiO_3$@TiO_2	75 W Xenon lamp	Rhodamine B	$3.14E^{-2}$	10	[3]
BiOBr@TiO_2	300 W Xe lamp	RhB	$2.50E^{-2}$	5	[4]
EPF(2/1)-TiO_2	4 W, 350−400 nm	Methylene blue	$5.02E^{-2}$	10	[5]
TiO_2-BN	365 nm	ibuprofen	$5.4E^{-2}$	8	[6]
TiO_2/g-C_3N_4	300 W Xe lamp	Rhodamine B	$6.4E^{-2}$	5	[7]
TiO_2/SnO_2	300 W medium Hg lamp	Methylene blue	$6.04E^{-2}$	3	[8]

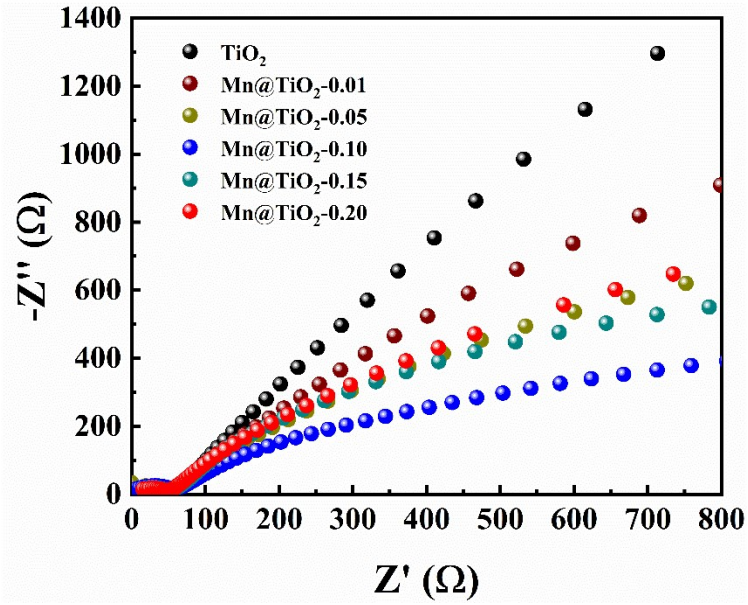

Figure SI 4: The electrochemical impendence spectroscopy (EIS) Nyquist plots of TiO_2, Mn@TiO_2-0.01; Mn@TiO_2-0.05; Mn@TiO_2-0.1; Mn@TiO_2-0.15, and Mn@TiO_2-0.20.

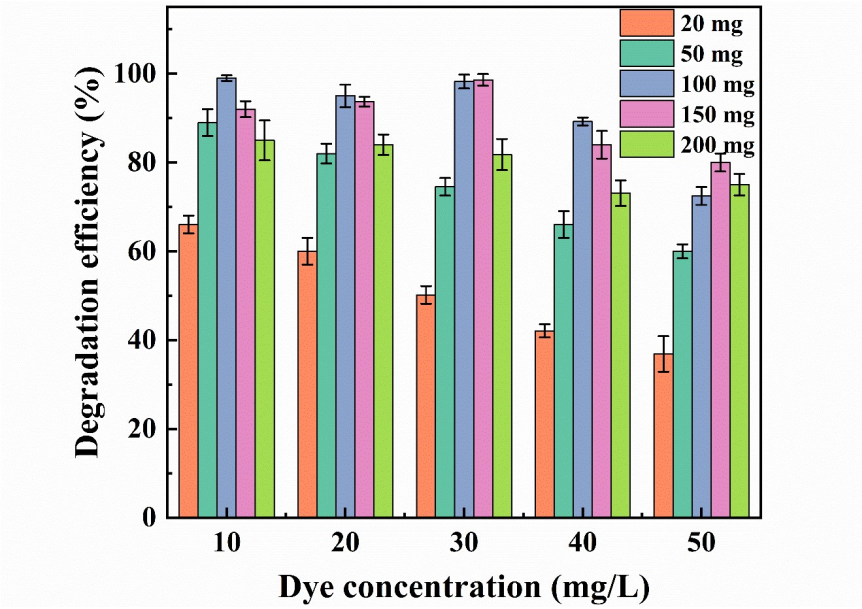

Figure SI 5: Effect of dye concentration and catalyst amount on the photodegradation efficiency of MB by Mn@TiO_2-0.10.

In order to explore the possibility of $Mn@TiO_2$ nanofilm applied for energy storage, the electron-chemical properties were investigated by a three-electrode system in 1 M Na_2SO_4 aqueous electrolyte, using a Pt counter electrode and an Hg/HgO reference electrode. Figure SI 1 displayed the cyclic voltammetry curve (CV) collected for $Mn@TiO_2$ nanofilm at different scan rates. These CV curves are all in the shape of a deformed rectangle, corresponding to the typical properties of the carbon-based electrochemical double-layer capacitors. From Figure SI 6 (b), the curve demonstrated a well rectangular-like curve no matter whether under at a low or higher scan speed testing, which implied good Faraday capacitance reaction has occurred on the film surface. As offered in Figure SI 6 (b), the charging and discharge curves of the $Mn@TiO_2$-0.10 were reasonably symmetric with a good linear relation of discharge/charge voltage versus time. This result again certificated the ideal capacitive characteristic and speedy charge/discharge property of $Mn@TiO_2$ samples. In order to measure the real-life performance of the prepared $Mn@TiO_2$, the charge and discharge cyclic stability was analyzed. After 5000 cycles, the capacitance still maintains 91 % of the initial capacitance as shown in Figure SI 6, exhibiting an excellent electrochemical stability. Besides, the charge and discharge curves are all in the shape of triangle as shown in Figure SI 6 (c) inset. Table SI 3 enumerated the mass-specific capacitance of all samples. The loading amounts of Mn^{4+} were comparable in these electrodes. As expected, the higher Mn^{4+} containing electrodes performed substantially larger current density owned to its higher electrochemically active. This also could be owing to the raised surface area and interior charge transport speed [9]. Therefore, all electrochemical result makes it is possible to foresee the improvement of TiO_2 conductivity as well as practice expanding.

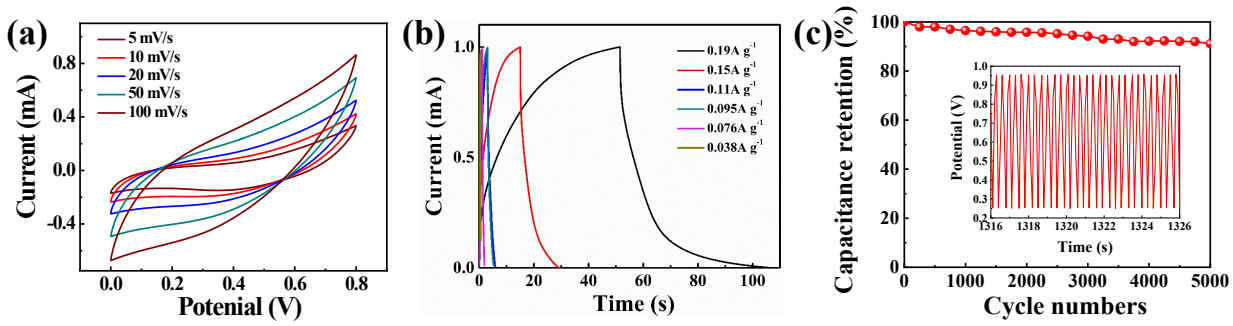

Figure SI 6: (a) CV curves collected of Mn@TiO_2-0.10 electrodes at the different scan rate; (b) Galvanostatic charge/discharge curves collected at different current densities for the sample operated within a voltage window of 1.0 V; (c) the long-term cyclic charge-discharge curve of Mn@TiO_2-0.10.

Table SI 3: mass specific capacitance of all samples.

Sample	Cm (F g^{-1})
TiO_2	1.11
Mn@TiO_2-0.01	2.69
Mn@TiO_2-0.05	4.13
Mn@TiO_2-0.10	5.09
Mn@TiO_2-0.15	8.07
Mn@TiO_2-0.20	8.37

References

1 H. Liu, Z.-G. Zhang, X.-X. Wang, G.-D. Nie, J. Zhang, S.-X. Zhang, N. Cao, S.-Y. Yan and Y.-Z. Long, *J. Phys. Chem. Solids*, 2018, **121**, 236–246.

2 M. Nasr, L. Soussan, R. Viter, C. Eid, R. Habchi, P. Miele and M. Bechelany, *New J. Chem.*, 2018, **42**, 1250–1259.

3 K. S. Ranjith and T. Uyar, *ACS Sustain. Chem. Eng.*, 2018, **6**, 12980–12992.

4 Y. Cai, J. Song, X. Liu, X. Yin, X. Li, J. Yu and B. Ding, *Environ. Sci. Nano*, 2018, **5**, 2631–2640.

5 C. G. Lee, H. Javed, D. Zhang, J. H. Kim, P. Westerhoff, Q. Li and P. J. J. Alvarez, *Environ. Sci. Technol.*, 2018, **52**, 4285–4293.

6 L. Lin, W. Jiang, M. Bechelany, M. Nasr, J. Jarvis, T. Schaub, R. R. Sapkota, P. Miele, H. Wang and P. Xu, *Chemosphere*, 2019, **220**, 921–929.

7 L. Cui, S. Liu, F. Wang, J. Li, Y. Song, Y. Sheng and H. Zou, *J. Alloys Compd.*, 2020, **826**, 154001.

8 L. Zhang, W. Yu, C. Han, J. Guo, Q. Zhang, H. Xie, Q. Shao, Z. Sun and Z. Guo, *J. Electrochem. Soc.*, 2017, **164**, H651–H656.

9 X. Lu, M. Yu, G. Wang, T. Zhai, S. Xie, Y. Ling, Y. Tong and Y. Li, *Adv. Mater.*, 2013, **25**, 267–272.